Hindawi Publishing Corporation
Advances in Materials Science and Engineering
Volume 2012, Article ID 168780, 9 pages
doi:10.1155/2012/168780

Research Article

Photocatalytic Degradation of Dichlorvos in Visible Light by Mg^{2+}-TiO_2 Nanocatalyst

T. Siva Rao,[1] Teshome Abdo Segne,[1] T. Susmitha,[1] A. Balaram Kiran,[1] and C. Subrahmanyam[2]

[1] *Department of Inorganic and Analytical Chemistry, School of Chemistry, Andhra University, Visakhapatnam 530003, India*
[2] *Department of Chemistry, Indian Institute of Technology Hyderabad, Hyderabad 500007, India*

Correspondence should be addressed to T. Siva Rao, raost@yahoo.com

Received 30 January 2012; Revised 8 March 2012; Accepted 19 March 2012

Academic Editor: Guohua Jiang

Photocatalytic activity of TiO_2 was studied by doping with magnesium (Mg^{2+}-TiO_2) with varying magnesium weight percentages ranging from 0.75–1.5 wt%. The doped and undoped samples were synthesized by sol-gel method and characterized by X-ray diffraction (XRD), N_2 adsorption-desorption (BET), X-ray photoelectron spectroscopy (XPS), UV-visible diffuse reflectance spectroscopy (DRS), and scanning electron microscopy (SEM). The XRD data has shown that anatase crystalline phase in Mg^{2+}-TiO_2 catalysts, indicating that Mg^{2+} ions did not influence the crystal patterns of TiO_2. The presence of magnesium ions in TiO_2 matrix has been determined by XPS spectra. DRS spectra showed that there is a significant absorption shift towards the visible region for doped TiO_2. The SEM images and BET results showed that doped catalyst has smaller particle size and highest surface area than undoped TiO_2. The photocatalytic efficiency of the synthesized catalysts was investigated by the photocatalytic degradation of aqueous dichlorvos (DDVP) under visible light irradiation, and it was found that the Mg^{2+}-doped catalysts have better catalytic activity than undoped TiO_2. This can be attributed that there is a more efficient electron-hole creation in Mg^{2+}-TiO_2 in visible light, contrary to undoped TiO_2 which can be excited only in UV irradiation. The effect of dopant concentration, pH of solution, dosage of catalysts, and initial pesticide concentration has been studied.

1. Introduction

Advanced oxidation process (AOP) is an alternative way of treating undesirable organic pollutants, including pesticides. According to the literature [1, 2] among AOPs, heterogeneous photocatalysis seems to be an attractive method and has been successfully employed for the degradation or transform into less harmful substances of various families of pollutants [3–5].

The photoinduced redox reactions have received an attention after the discovery of first photoelectrochemical splitting of water on titanium dioxide electrode by Fujishima and Honda [6]. Later, many novel redox reactions of organic and inorganic substrates have been induced by band-gap irradiation of a variety of semiconductor particles [7, 8]. There are a lot of different semiconductor materials which are readily available (e.g., TiO_2, ZnO, Fe_2O_3, CdS, and ZnS), but only a few are suitable for sensitizing the photomineralization of a wide range of organic pollutants. A sensitizer for reaction must be [9, 10] (i) photoactive, (ii) able to utilize visible and/or near the UV light, (iii) biologically and chemically inert, and (iv) photostable.

Among various semiconductor photocatalysts available, TiO_2 has attracted a great deal of study for its high photocatalytic activity, nontoxic property, chemical stability, and highest oxidation rate of many photoactive metal oxides investigated [11]. TiO_2 is capable of decomposing a wide range of organic, inorganic, and toxic pollutants [12].

Although TiO_2 is superior to other semiconductors for many practical uses, two types of defects limit its photocatalytic activity. Firstly, TiO_2 has high bandgap energy (3.2 eV), which is only 4-5% of the overall solar spectrum. Thus this restricts the use of visible light. Secondly, the high rate of electron-hole recombination at TiO_2 particles results in low photoquantum efficiency [13]. In order to overcome these limitations of TiO_2, many attempts have been made to prepare different types of TiO_2 by depositing of noble metals, mixing metal oxides, surface derivatization, and doping

selective metal ions into TiO_2 [14, 15], and also Graphene-based semiconductor photocatalysts are prepared [16].

The addition of low percentage of metal by doping was often proposed to improve the photocatalytic activity of TiO_2. The advantage of doping the metal ions into TiO_2 is the temporary trapping of the photogenerated charge carriers by the dopant and the inhibition of their recombination during migration from the inside of the material to the surface, by modifying the bandgap of the photocatalyst. A wide range of metal ions have been studied for doping TiO_2 and their effects on the properties of TiO_2 and on its photocatalysis [17, 18], but reports on alkaline-earth metal ions doping into TiO_2 and their photocatalytic properties have seldom been seen.

Sol-gel process is one of the versatile, simple, and easy means of synthesizing nanosize materials in contrast to the other conventional preparation methods which do not usually produce homogeneous, high-surface-area materials. The main advantage of the sol-gel method in preparing catalytic materials is its excellent control over the properties of the product via a host of parameters that are accessible in all four key processing steps: formation of a gel, aging, drying, and heat treatment. Although titania catalysts have been extensively studied, the procedure of preparing photocatalytic metal-doped titania is still of great interest.

Waste waters generated from the agricultural application of dichlorvos contain the residue of dichlorvos which has been evaluated in a wide range of toxicology assays including bioassays for carcinogenicity and mutagenicity (genotoxicity) [19, 20]. It is also more likely to contaminate surface and ground waters due to its high solubility in water. This could have an adverse effect on the aquatic environment, and procedure has to be found for its degradation. Electron transfer process occurring between pesticide and semiconductor, especially TiO_2, has been examined and found to have practical potential [21].

The present paper has been focused to develop a visible light response catalyst via magnesium-doped titanium dioxide in varying percentages of metal. Characterization has been carried out using XRD, BET, XPS, DRS, and SEM. The photocatalytic activities of the synthesized samples have been evaluated by the degradation of a representative model pesticide pollutant, dichlorvos.

2. Experimental

2.1. Preparation of Photocatalysts. Titanium tetra-n-butoxide [$Ti(O\text{-}Bu)_4$] and magnesium nitrate were obtained from E. Merck (Germany) and used as titanium and magnesium sources for preparing anatase TiO_2 and Mg^{2+}-TiO_2 photo catalysts. Aqueous dichlorvos solution was used as a model compound for degradation. All other chemicals used in this work are of analytical grade, and doubly distilled water was used for the solution preparation.

Mg^{2+}-TiO_2 samples were prepared by sol-gel method in which initially a solution containing 40 mL of absolute alcohol, 6 mL of H_2O, and magnesium nitrate with required percentages (0.75 wt.%, 1.00 wt.%, 1.25 wt.% and 1.50 wt.%) was prepared (solution I). Another solution was prepared by taking 21 mL of $Ti(O\text{-}Bu)_4$ in 40 mL of absolute alcohol with stirring for 10 minutes, and then 3 mL of HNO_3 was added dropwise under continuous stirring for 30 minutes (solution II). Solution I was added to solution II slowly from the burette with vigorous stirring at room temperature until the transparent sol was obtained, and the resulting sol was further stirred for 1 h. The gel was prepared by aging the solution for 48 h at room temperature. The derived gel was dried at 100°C in an oven and ground. The catalyst powder was calcined at 400°C in furnace for 2 h. Undoped TiO_2 is also prepared with same procedure without metal nitrate. The doping concentrations are expressed as weight percentage of titanium atom. The powders are stored in black coated air-tight glass containers.

2.2. Characterization of Photocatalysts. The crystal phase composition of the prepared photocatalysts (TiO_2, Mg^{2+}-TiO_2) was determined by X-ray diffraction measurement carried out at room temperature using a PANalytical, D/Max-III A diffractometer with CuK_α radiation (λ = 0.15148 nm) with a liquid nitrogen gas-cooled germanium solid-state detector. The accelerating voltage of 35 kV and emission current of 30 mA were used and studied in the range of 2°–90° 2θ with a step time of 2° min^{-1}. The Brunauer-Emmett-Teller (BET) surface area was determined from the N_2 adsorption-desorption isotherm at 77.3 K by using a Quantachrome Nova 2200 E system. The sample was outgassed for 3 h at 300°C prior to the adsorption. The specific surface area was determined by using the standard BET method. To study the valence state of the photocatalysts, X-ray photoelectron spectroscopy (XPS) was recorded with the PHI quantum ESCA microprobe system, using the AlK_α line of a 250 W X-ray tube as a radiation source with the energy of 1486.6 eV, 16 mA × 12.5 kV, and a working pressure lower than 1×10^{-8} Nm^{-2}. As an internal reference for the absolute binding energies, the C 1s peak of hydrocarbon contamination was used as reference to 284.8 eV. The fitting of XPS curves was analyzed with MultiPak 6.0 A software. The DRS were recorded with a Shimadzu 3600 UV-visible NIR spectrophotometer equipped with an integrating sphere diffuse reflectance accessory, using $BaSO_4$ as reference scatter. Powder samples were loaded into a quartz cell, and spectra were recorded in the range of 200–900 nm. The morphology and size of particles was characterized using SEM (JSM-6610 LV) spectrophotometer and operated at 20 kV. A Horiba Jobin FluoroMax-4 instrument has been used for the PL, spectral data analysis, with a PMT voltage was 150 V and with slit set both at 2.5 nm.

2.3. Photocatalytic Activity of the Catalysts. Photocatalytic degradation studies of DDVP were carried out in a modified photoreactor system, in which 100 mL of reaction mixture illuminated with 400 W high-pressure mercury vapor lamp (Osram, India). The distance between the light source and the reaction beaker was 20 cm. Prior to irradiation, the solution with catalyst was stirred in the dark for 45 min to ensure establishment of adsorption-desorption equilibrium

of dichlorvos on catalyst surface. Aliquots of the samples were withdrawn from the solution by using Millipore syringe (0.45 μm) at certain time intervals and analyzed for dichlorvos concentration. The quantitative determination of DDVP was performed by measuring the absorption of phosphate ion formed at 465 nm with a Milton-Roy spectronic-1201 UV-visible spectrometer. The IR (>700 nm) and UV (<360 nm) radiations were filtered by water and UV filters, respectively.

Previous studies have shown that the photocatalytic degradation of pesticides by irradiating with UV light source and using TiO_2 or ZnO as catalyst leads to the formation of H^+, Cl^-, PO_4^{3-}, and CO_2 as final products, and their formation during the progress of the degradation of DDVP was confirmed by simple qualitative analysis tests. PO_4^{3-} was determined calorimetrically by the molybdenum blue method:

$$(CH_3O)_2POOCHCCl_2 + \left(\frac{9}{2}\right)O_2 \longrightarrow PO_4^{3-} + 4CO_2 + 2\ Cl^- + 5\ H^+ + H_2O. \quad (1)$$

Hence, in order to study the extent of mineralization of DDVP over illuminated Mg^{2+}-doped TiO_2, the absorbance measurements of PO_4^{3-} were carried out. The percentage of degradation was calculated from the following equation:

$$\%\ \text{Phosphate ion formation} = \left[\frac{A_t}{A_0}\right] \times 100, \quad (2)$$

where A_0 is calculated concentration of phosphate ion of the corresponding concentration and A_t is absorbance at time t.

3. Results and Discussions

3.1. XRD Diffraction Study and BET Results. The crystalline phases of the synthesized TiO_2 and Mg^{2+}-TiO_2 were examined by XRD, and the diffractograms are given in Figure 1. The XRD patterns of calcined (400°C) TiO_2 and the samples of Mg^{2+}-TiO_2 (Mg/Ti = 0.75, 1.0 and 1.25 wt.%) show only anatase form, indicating that Mg^{2+} ions in TiO_2 did not influence the crystal patterns of TiO_2 particle. Further, examination of XRD patterns of both pure and Mg^{2+}-doped TiO_2 illustrates the existence of peaks at 25.3, 37.7, 47.7, and 54.2 (2θ). The intensity of anatase TiO_2 peaks increased due to doping, and peaks corresponding to $MgNO_3$ and $MgCO_3$ were not detected. This may be due to the well dispersion of Mg^{2+} content in TiO_2 particles.

Since Mg^{2+} is more electropositive, the electronic cloud in each TiO_2 might be loosely held, favoring the formation of less dense anatase phase. In other words, the tight packing arrangement required for rutile phase formation is fully suppressed by the addition of magnesium nitrate in water which enhances the polarity of water, thus facilitating the formation of anatase phase exclusively. In addition, the presence of residual alkyl groups can also reduce the rate of crystallization of TiO_2 which favored the formation of less dense anatase phase.

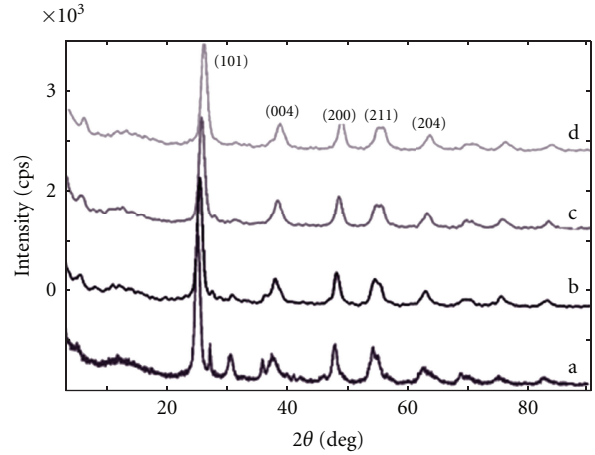

Figure 1: XRD patterns of (a) undoped TiO_2, (b) 0.75 wt.% of Mg^{2+}-doped TiO_2, (c) 1.0 wt.% of Mg^{2+}-doped TiO_2, and (d) 1.25 wt.% of Mg^{2+}-doped TiO_2.

The BET surface area results have shown that there is a much increase in surface area of doped catalysts than undoped one. With the incorporation of Mg^{2+} dopant during the sol-gel preparation technique, there was crystal growth suppression, favoring the formation of smaller TiO_2 crystallite. This effect may be attributed to the enhanced lattice strain in the doped TiO_2 network and then decrease grain growth rate.

3.2. Diffuse Reflectance Spectroscopy. The DRS of Mg^{2+}-doped TiO_2 and undoped TiO_2 samples are given in Figure 2. The spectra of undoped TiO_2 showed an absorption peak at 388 nm in the UV region. The absorption peak of the doped TiO_2 with different percentages of Mg^{2+} at 0.75 wt.%, 1.0 wt.%, 1.25 wt.%, and 1.50 wt.% shows considerable shift towards the visible region at around 400–800 nm for all the samples. The tailing absorption peaks can be considered as the extra tail states in the bandgap because Mg^{2+} was added to the TiO_2 matrix. The extension of absorption edge to longer wavelengths for Mg^{2+}/TiO_2 indicates the existence of good contact between TiO_2 and the metal (Mg^{2+}) ion grain.

The UV-Vis absorption edge and bandgap energies of the samples were determined from the reflectance [F(R)] spectra using the Kubelka-Munk (KM) formalism and the Tauc plot method [22]. The extrapolated lines for Mg^{2+}-doped TiO_2 have been given in Figure 3 and used to determine the bandgap energies for Mg^{2+}-doped TiO_2, undoped TiO_2, and Degussa P25 samples. The calculated bandgap energies are given in Table 1. The largest reduction gap is observed for catalyst containing 1.25 wt.% of Mg^{2+}-doped TiO_2. This reduction bandgap may be attributed to the doping of Mg^{2+} as impurity into the host structure (TiO_2) and create extra energy levels situated within the bandgap [23]. The extra energy level created within the bandgap due to shifting of the Fermi energy level of Mg^{2+} towards valence band since metal create P-type semiconductor.

Table 1: Crystallite size, BET surface area, and bandgap energy of each catalyst.

Catalyst no.	wt.% doping of Mg^{2+} in TiO_2	Calcination temp. (°C)	Crystallite size (nm)	BET surface area (m^2/g)	Bandgap energy (eV)
(1)	0.75	400	15.00	85.209	2.90
(2)	1.0	400	12.11	105.987	2.85
(3)	1.25	400	11.25	107.267	2.75
(4)	1.50	400	13.26	101.820	2.95
(5)	Undoped TiO_2	400	11.30	79.382	3.2
(6)	Degussa P25	—	—	69.962	3.1

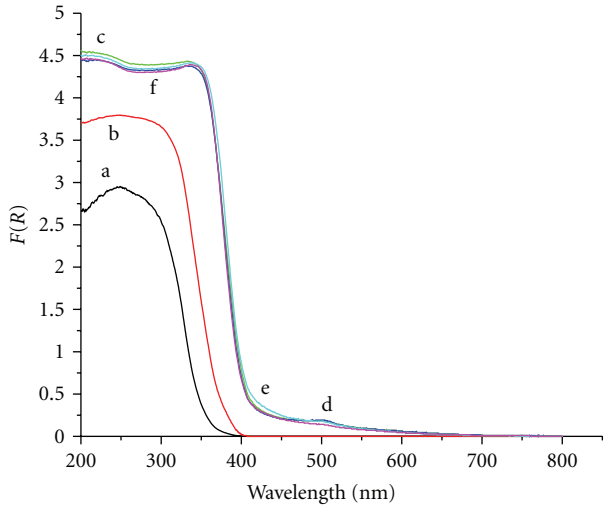

(a) Undoped TiO_2
(b) Degussa P25
(c) 0.75 wt.% of Mg^{2+}
(d) 1 wt.% of Mg^{2+}
(e) 1.25 wt.% of Mg^{2+}
(f) 1.5 wt.% of Mg^{2+}

Figure 2: The DRS-UV-Vis spectra of Degussa P25, undoped, and doped TiO_2 with different % of Mg^{2+}.

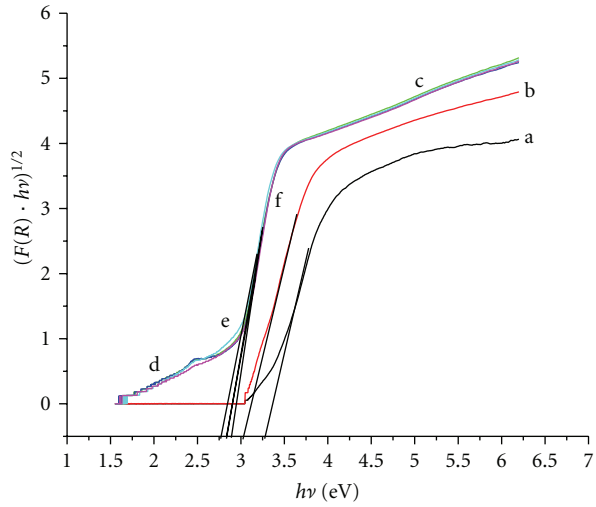

(a) Undoped TiO_2
(b) Degussa P25
(c) 0.75 wt.% of Mg^{2+}
(d) 1 wt.% of Mg^{2+}
(e) 1.25 wt.% of Mg^{2+}
(f) 1.5 wt.% of Mg^{2+}

Figure 3: Plots of transformed Kubelka-Munk functions $[F(R)\cdots \mathrm{h}\nu]^{1/2}$ versus hν for Degussa P25, undoped TiO_2, and Mg^{2+}-doped TiO_2 samples.

3.3. BET Surface Areas and Pore Distribution. The BET surface areas of the as-prepared Mg^{2+}-TiO_2 sample have been given in Table 1, and nitrogen adsorption and desorption isotherms and corresponding pore size distribution curves (inset) are given in Figure 4. It is observed that at relatively high pressures between 0.075 and 0.15 (P/P_o), the curve exhibit a hysteresis loop indicating the presence of mesopores. The shape of the hysteresis loop is of type H3, associated with particle giving rise to narrow slit shaped pores [24–27]. From Figure 4 the inset figure indicated the pore size distribution range from 20 to 35 nm. The pore volume of the as-prepared catalyst is 0.135 m^3/g. However, the existing poresarise maybe due to removal of nitrate ion and organic moiety from the metal precursors (magnesium and titanium). Due tothis, organized porous structure within the bulk sample of the catalyst may helpful in photocatalysis.

3.4. Analysis of Hydroxyl Radicals ($OH^{\bullet}$). The analysis of hydroxyl radicals has been carried out by photoluminescence technique [28]. 0.1 g of Mg^{2+}-TiO_2 in 10 ppm of coumarin solution was illuminated with visible light. The fluorescence emission spectrum excited at 428 nm from the coumarin solution was measured at every 15 min of illumination. Figure 5 shows the induction of fluorescence from 10 ppm coumarin solution. As shown in the figure, gradual increase in the fluorescence at about 500 nm for 7-hydroxycoumarin which is obtained due to reaction of OH radicals and coumarin was observed by continuous illumination of visible light on the Mg^{2+}-TiO_2 solution. The trend observed in the figure indicated that formation of the OH radicals is proportional to the irradiation time.

3.5. XPS Measurements. X-ray photoelectron spectroscopy (XPS) analysis of magnesium- (II) doped sample was performed, and high-resolution scans are shown in Figures 6(a), 6(b), and 6(c). The XPS observations show that only Mg, Ti and O elements were detected from the samples in spectrum analysis. The binding energy of Mg 2p was found

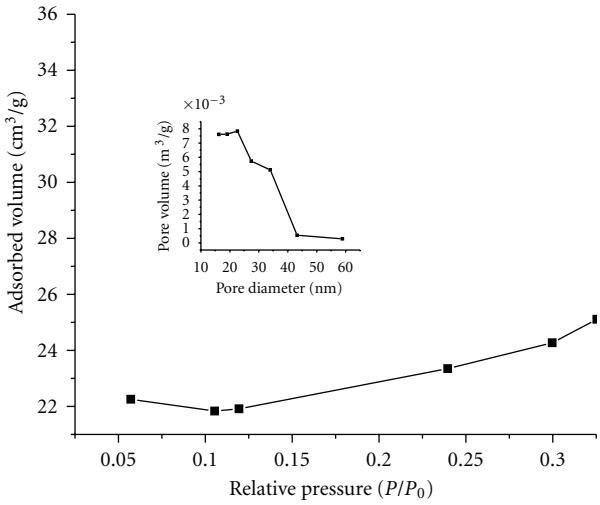

Figure 4: Nitrogen adsorption-desorption isotherms and corresponding pore size distribution. Curves (inset) of the Mg^{2+}-TiO_2 prepared at 1.25 wt.% of Mg^{2+}.

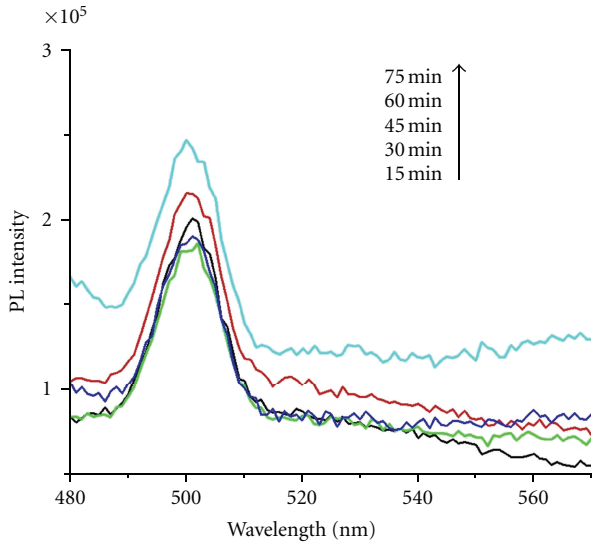

Figure 5: PL spectral changes with irradiation time on the undoped TiO_2 and 10 ppm coumarin.

to be 50.4 eV (Figure 4(a)) which is a typical of Mg^{2+} that bonded to oxygen and was assigned to the compound MgO. The binding energies of Ti $2p_{3/2}$ and Ti $2p_{1/2}$ were found to be 458.4 and 464.0 eV, and these bands could belong to Ti^{4+} (Figure 6(b)) and there was no fitting peak for Ti^{3+}. Hence the XPS-spectra confirmed the chemical composition of magnesium-doped sample to be MgO and TiO_2.

3.6. Scanning Electron Microscopy. The SEM images of TiO_2 and metal-doped TiO_2 catalysts are shown in Figures 7(a) and 7(b). The image of samples containing 1.25 wt.% of Mg^{2+} ion shows the morphological changes induced by the addition of alkaline earth cation. The catalysts are found to

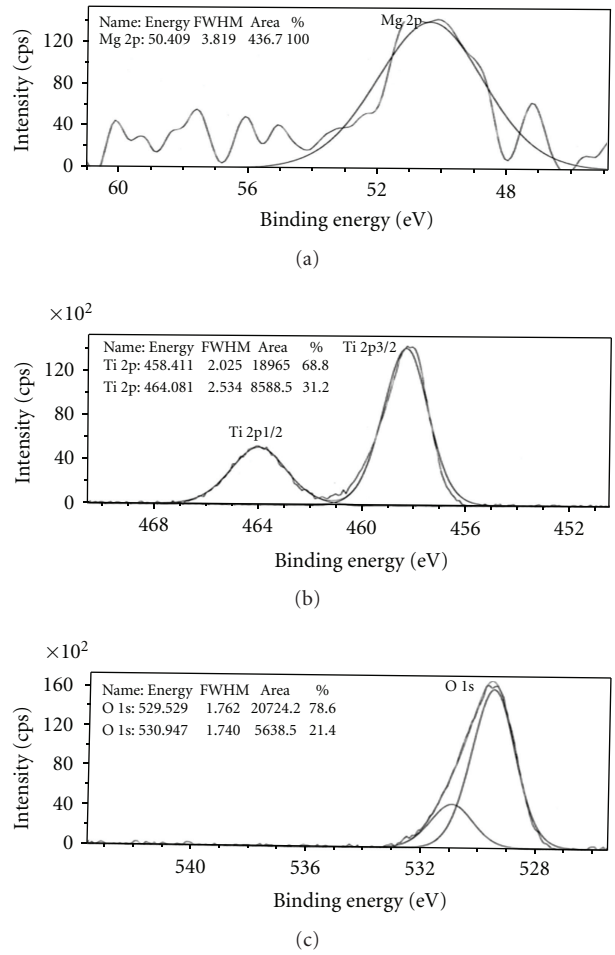

Figure 6: (a) High resolution of Mg 2p spectrum, (b) high resolution of Ti 2p spectrum, and (c) high resolution of O 1s spectrum.

contain irregular-shaped particles which are again aggregates of tiny crystals. Figure 7(a) shows anatase (undoped TiO_2) produced with no addition of magnesium ion. The sample appears as large blocks of coarse material of dimensions from around 1 to 20 μm. Figure 7(b) shows sample containing 1.25 wt.% of Mg^{2+}, with reduction in the particle size to 1–10 μm range. This clearly illustrates the altered morphology of the catalyst powders, which consists of a large portion of submicron-sized particles.

3.7. FT-IR Spectral Study. FT-IR spectra of undoped TiO_2 and 1.25 wt.% of Mg^{2+}-TiO_2 given in Figures 8(a) and 8(b) have shown peaks corresponding to stretching vibrations of O–H and bending vibrations of adsorbed water molecules around 2322–3317 cm^{-1} and 1613 cm^{-1}, respectively. The intensity of the peaks became less in Mg^{2+}-TiO_2, indicating the removal of large portion of adsorbed water from TiO_2.

The broad band below 456.06 cm^{-1} of undoped TiO_2 is due to Ti–O–Ti vibration. This peak has been shifted to 470.63 cm^{-1} in Mg-doped TiO_2 which may be because of Ti–O–Mg vibration. Hence the FT-IR spectral study along with XPS established the substitution of Mg^{2+} into TiO_2 lattice.

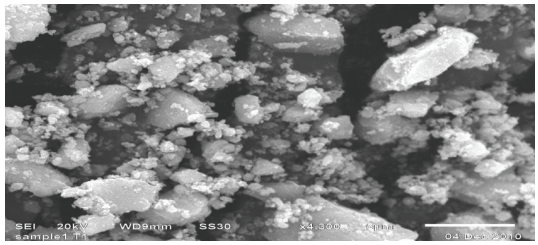

(a)

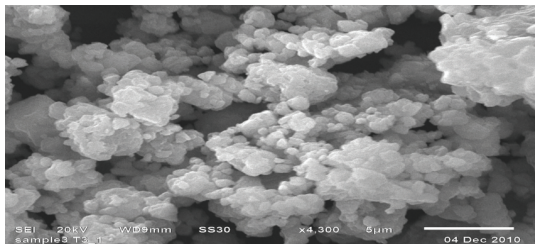

(b)

Figure 7: SEM images of (a) undoped TiO_2 and (b) 1.25 wt.% of Mg-doped TiO_2.

3.8. Photocatalytic Degradation of Dichlorvos. To understand the photocatalytic activity of the prepared catalysts, degradation of dichlorvos pesticide under the irradiation of visible light has been carried out, in the presence and absence of catalysts. The percentage of DDVP degradation is significantly less in the absence of catalyst (0.05% for 9 hours irradiation) when compared to that of undoped or doped titanium dioxide. A blank experiment in the absence of irradiation along with catalysts demonstrated that no significant change in the DDVP concentration was observed. The efficiency of photocatalytic degradation process depends on various experimental parameters such as effect of dopant concentration, pH, catalyst dosage, and initial concentration of pollutant. Hence, it is essential to optimize these parameters to achieve higher degradation efficiency of photocatalyst.

3.8.1. Effect of Mg Dopant Concentration on Photocatalytic Degradation of DDVP. Figure 9 shows the results of the photocatalytic degradation of DDVP by irradiation of visible light over Degussa P25, undoped TiO_2 catalyst, and Mg-doped TiO_2 photocatalyst with different doping concentrations of Mg in TiO_2. Among various concentrations of Mg, 1.25 wt.% of Mg-TiO_2 catalyst exhibits the highest photocatalytic activity. This may be attributed to that increase in dopant concentration leads to increase in number of trapped charge carriers per particle [15, 29] and is the highest in 1.25 wt.% of Mg^{2+}-TiO_2 which is the optimum concentration showing maximum photocatalytic activity.

The results of the experiment show that the rate of phosphate ion formation increased with increase in the concentration of magnesium ions, and it was optimum at 1.25 wt.%. However, magnesium ions' doping became detrimental when the dopant concentration was above 1.25 wt.%.

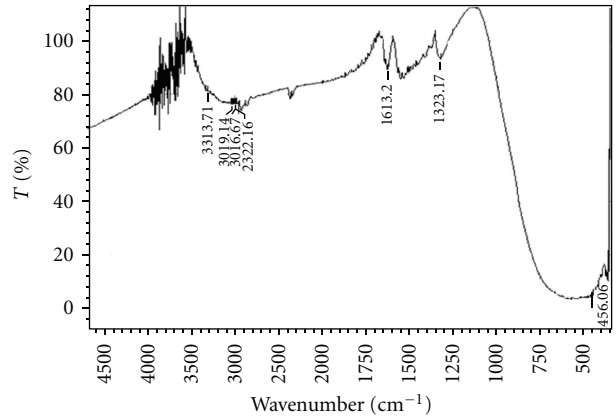

(a)

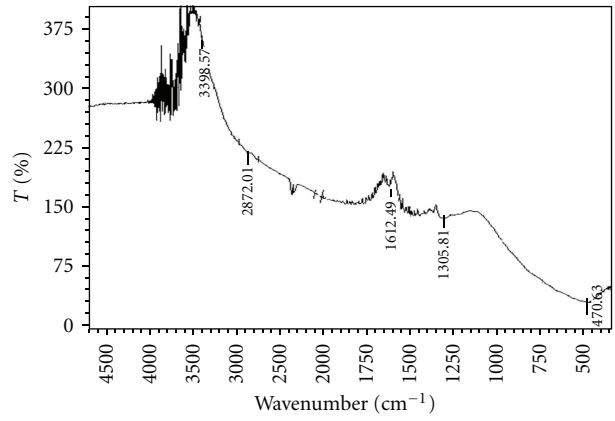

(b)

Figure 8: FT-IR spectra of (a) undoped TiO_2 and (b) 1.25 wt.% Mg^{+2}-TiO_2.

It also demonstrates that, even though the concentration of the doped magnesium ions is small, it still gives much influence on the photocatalytic activity of TiO_2 particles.

3.8.2. Effect of pH. The adsorption properties of catalysts can be greatly changed at different pH values; hence, the catalyst-assisted photodegradation of DDVP has also been monitored by in situ measurements of pH of the aqueous solution with irradiation time, at a fixed weight of catalyst and DDVP pesticide concentration at different pH values. Solution pH influences adsorption and desorption of the substrate, catalyst surface charge, oxidation potential of the valence band, and other physicochemical properties.

The effect of pH on the photocatalytic degradation of DDVP is shown in Figure 10. The degradation plot for DDVP has been plotted between rate constant and pH of the solution. Based on the results, it is observed that the rate of degradation decreased with increase in pH of the solution. The optimum pH of the solution for the degradation of DDVP is 2. Generally in acidic pH the surface of the TiO_2 is in the form of $TiOH_2^+$. The photogenerated electrons can be captured by the adsorbed H^+ to form $H^{\bullet}_{ads}$. At higher pH,

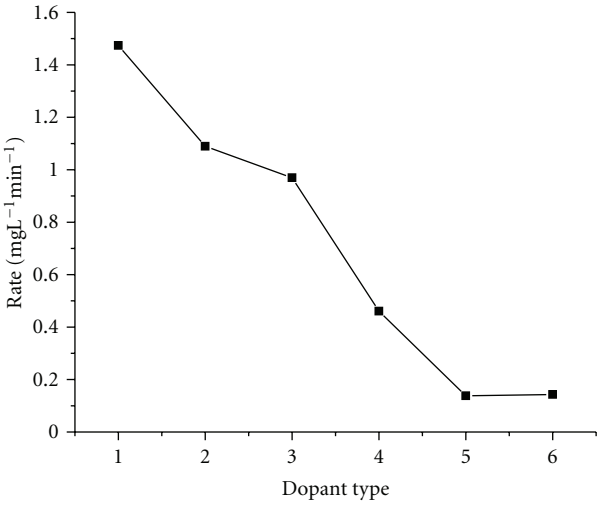

Figure 9: Effect of dopant concentration on the degradation of dichlorvos. Catalyst dosage = 0.10 g, pH = 3, and [DDVP] = 150 ppm.

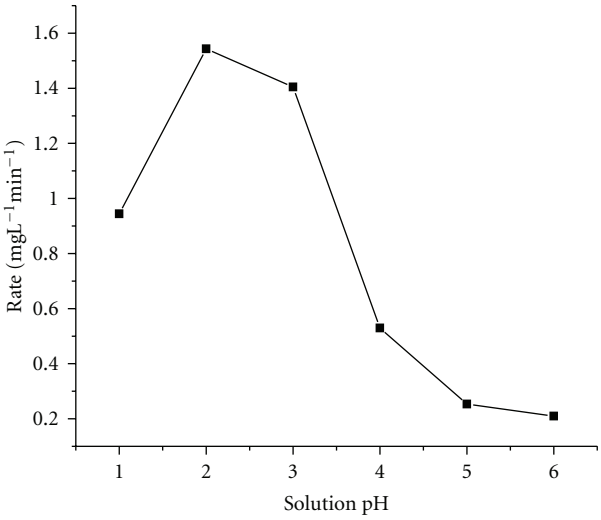

Figure 10: The effect of pH on the degradation of dichlorvos by Mg^{2+}-doped TiO_2. Catalyst dosage = 0.10 g, [DDVP] = 150 ppm.

the surface of catalyst has a net negative charge as TiO_2^-, and hence the degradation rate was found to be lower:

$$\begin{aligned} \mathrm{TiOH} + \mathrm{H^+} &\longrightarrow \mathrm{TiOH_2^+}, \quad \mathrm{pH} < 6.25, \\ \mathrm{TiOH} &\longrightarrow \mathrm{TiO^-} + \mathrm{H^+}, \quad \mathrm{pH} > 6.25. \end{aligned} \tag{3}$$

3.8.3. Effect of Catalyst Dosage. The effect of the amount of catalyst on the photodegradation rate was investigated at a fixed pH and initial concentration of the dichlorvos, experiments were performed with varying amounts of Mg^{2+}-TiO_2 from 0.025 g to 0.3 g in 100 mL DDVP pesticide aqueous solution. The degradation pattern from such experiments has been depicted in Figure 11, which reveals that the rate of degradation increases linearly with increase in the amount of catalyst up to 0.1 g and then decreases. This may be explained by two main reasons. The first one is due to the presence of foreign metal ions (Mg^{2+}) as dopant that helps in inhibiting electron-hole pair recombination and enhancing interfacial charge transfer reactions, which leads to increased catalytic activity.

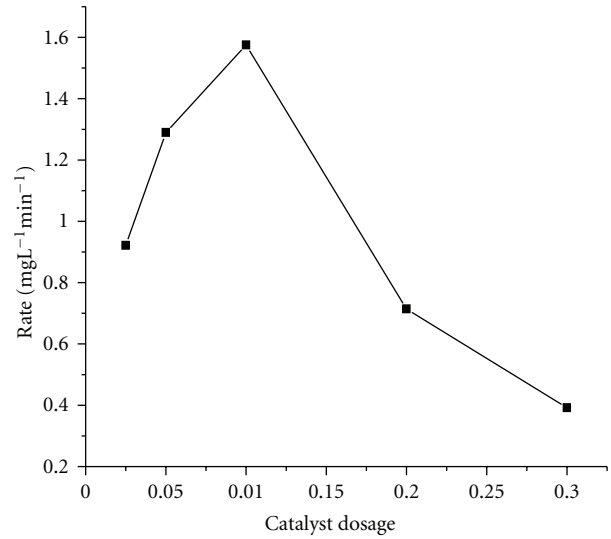

Figure 11: The effect of catalyst dosage on the degradation of dichlorvos by Mg^{2+}-doped TiO_2, pH = 2, [DDVP] = 150 ppm.

Secondly, as the amount of catalyst increases, the number of photons absorbed and the number of DDVP molecules adsorbed are increased leading to the increase in DDVP degradation. At higher concentrations of catalyst, although more surface areas are available for constant DDVP molecules, the solution turbidity increases and it interferes with the penetration of light. The deactivation of activated molecules by collision with ground-state molecules may also hinder the photocatalytic efficiency [30]. Hence, above a certain level, additional catalyst amount is not involved in catalysis, and thus the rate levels off.

3.8.4. Effect of Initial Pesticide Concentration. At a fixed weight of Mg^{2+}-TiO_2 and pH, variation of initial pesticide concentration on photo degradation was studied and shown in Figure 12. It was noted that the degradation rate increases with the increase of pesticide concentration up to a certain concentration (150 ppm), and a further increase leads to a decrease in the pesticide degradation rate. This is due to the reduction of generation of radicals ($OH^\bullet$) on the catalyst surface since the active surfaces are covered by pesticide molecules.

3.9. Photocatalytic Mechanism. Based on the experimental results and reports of the previous workers, the following

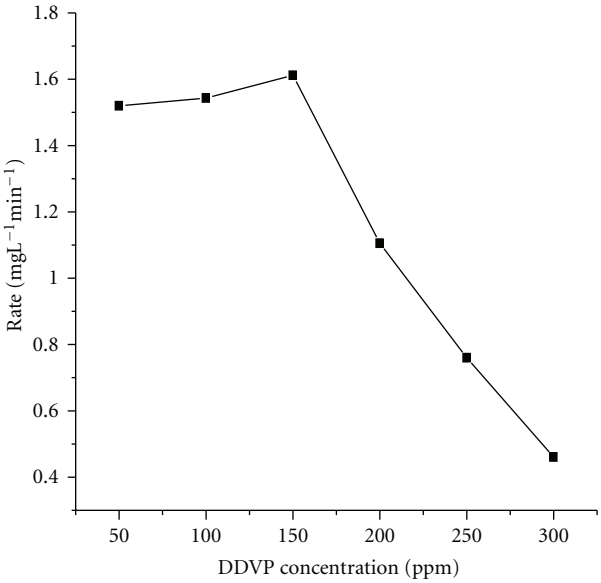

Figure 12: The effect of concentration of DDVP on the degradation of dichlorvos by Mg^{2+}-doped TiO_2, pH = 2, catalyst dosage = 0.10 g.

mechanism would be proposed for the photocatalytic reactions of magnesium-doped TiO_2 [31–33].

(a) Upon visible light illumination of photocatalyst, electrons are ejected from the valence band to the conduction band leaving positive holes in the valence band.

(b) When the metal ion doped into TiO_2 lattice, it trapped the ejected electrons, holding up the recombination process.

(c) The trapped electrons can be further scavenged by molecular oxygen, which is adsorbed on the TiO_2 surface to generate superoxide radical, and this in turn produces hydrogen peroxide (H_2O_2), hydroperoxy ($HO_2^{\bullet}$), and hydroxyl ($^{\bullet}OH$) radicals.

(d) The positive holes in the valence band act as good oxidizing agents available for degradation of pesticide in the solution. Thus, the DDVP is attacked by the hydroxyl radicals formed both by trapped electrons and hole in the VB as given in the above equations, to generate phosphate ions, organic radicals, or other intermediates, which further undergo degradation.

4. Conclusions

The DRS analysis shows that doping of Mg^{2+} into TiO_2 shifts the absorbance band of TiO_2 from UV to visible region, and the bandgap energy is reduced for all doped catalysts (from 3.2 eV to 2.75 eV); the largest reduction gap was observed for doped catalyst of 1.25 wt.% of Mg. The incorporation of Mg^{2+} ions into the TiO_2 was evidenced by XPS analysis. The BET results also show that there is an increase in surface area of the catalyst, which enhances the photocatalytic degradation of DDVP in visible light. The present work imparts the significance of magnesium ion doping into titania, in dichlorvos degradation. It also establishes the doping of magnesium by sol-gel as a best alternative method. The experimental results show that the photocatalytic activity of undoped TiO_2 is lower than magnesium-doped TiO_2.

Magnesium doping causes better separation of electron and holes on the modified TiO_2 surface allowing more efficient channeling of the produced electrons into useful redox reactions, thus enhancing the DDVP degradation in the presence of visible light, when compared to undoped TiO_2 which can be excited only in less available UV light. The degradation of DDVP was maximum at 150 ppm DDVP concentration, 0.1 g of Mg^{2+}-TiO_2 catalyst, and at a pH of 2 using 1.25 wt.% of magnesium-doped titania catalyst.

Acknowledgments

T. Rao and Mrs. T. Susmitha are thankful to UGC, New Delhi, for financial assistance as major research project to carry out research work and also thankful to Dr. Sridhar, Scientist, IICT, Hyderabad, for providing XPS spectral data. T. A. Segne is also thankful to the Ethiopian Government for their financial support for doing Ph.D. at the Andhra University, Visakhapatnam, India.

References

[1] O. Legrini, E. Oliveros, and A. M. Braun, "Photochemical processes for water treatment," *Chemical Reviews*, vol. 93, no. 2, pp. 671–698, 1993.

[2] D. Chen and A. K. Ray, "Photocatalytic kinetics of phenol and its derivatives over UV irradiated TiO_2 ," *Applied Catalysis B*, vol. 23, no. 2-3, pp. 143–157, 1999.

[3] A. L. Linsebigler, G. Lu, and J. T. Yates, "Photocatalysis on TiO_2 surfaces: principles, mechanisms, and selected results," *Chemical Reviews*, vol. 95, no. 3, pp. 735–758, 1995.

[4] C. Minero, E. Pelizetti, P. Pichat, M. Sega, and M. Vincenti, "Formation of condensation products in advanced oxidation technologies: the photocatalytic degradation of dichlorophenols on TiO_2 ," *Environmental Science and Technology*, vol. 29, no. 9, pp. 2226–2234, 1995.

[5] P. K. J. Robertson, "Semiconductor photocatalysis: an environmentally acceptable alternative production technique and effluent treatment process," *Journal of Cleaner Production*, vol. 4, no. 3, pp. 203–212, 1996.

[6] A. Fujishima and K. Honda, "Electrochemical photolysis of water at a semiconductor electrode," *Nature*, vol. 238, no. 5358, pp. 37–38, 1972.

[7] R. W. Matthews, "Photooxidation of organic impurities in water using thin films of titanium dioxide," *Journal of Physical Chemistry*, vol. 91, no. 12, pp. 3328–3333, 1987.

[8] M. A. Fox, C. C. Chen, K. Park, and J. N. Younathan, "Controlled organic redox reactivity on irradiated semiconductor surfaces," *ACS Symposium Series*, vol. 278, pp. 69–78, 1985.

[9] A. Mills, R. H. Davies, and D. Worsley, "Water purification by semiconductor photocatalysis," *Chemical Society Reviews*, vol. 22, no. 6, pp. 417–425, 1993.

[10] S. Peng, Y. Li, F. Jiang, G. Lu, and S. Li, "Effect of Be^{2+} doping TiO_2 on its photocatalytic activity," *Chemical Physics Letters*, vol. 398, no. 1–3, pp. 235–239, 2004.

[11] M. R. Hoffmann, S. T. Martin, W. Choi, and D. W. Bahnemann, "Environmental applications of semiconductor photocatalysis," *Chemical Reviews*, vol. 95, no. 1, pp. 69–96, 1995.

[12] Y. Ku, W. Wang, and Y. S. Shen, "Reaction behaviors of decomposition of monocrotophos in aqueous solution by UV and UV/O_3 processes," *Journal of Hazardous Materials*, vol. 72, no. 1, pp. 25–37, 2000.

[13] C. Kormann, D. W. Bahnemann, and M. R. Hoffmann, "Preparation and characterization of quantum-size titanium dioxide," *Journal of Physical Chemistry*, vol. 92, no. 18, pp. 5196–5201, 1988.

[14] J. Moser and M. Grätzel, "Photosensitized electron injection in colloidal semiconductors," *Journal of the American Chemical Society*, vol. 106, no. 22, pp. 6557–6564, 1984.

[15] W. Choi, A. Termin, and M. R. Hoffmann, "The role of metal ion dopants in quantum-sized TiO_2: correlation between photoreactivity and charge carrier recombination dynamics," *Journal of Physical Chemistry*, vol. 98, no. 51, pp. 13669–13679, 1994.

[16] Q. Xiang, J. Yu, and M. Jaroniec, "Graphene based semiconductor photocatalysis," *Chemical Society Reviews*, vol. 41, no. 2, pp. 782–796, 2012.

[17] Y. Bessekhouad, D. Robert, J. V. Weber, and N. Chaoui, "Effect of alkaline-doped TiO_2 on photocatalytic efficiency," *Journal of Photochemistry and Photobiology A*, vol. 167, no. 1, pp. 49–57, 2004.

[18] S. Liu, J. Yu, and M. Jaroniec, "Anatase TiO_2 with dominant high-energy {001} facets: synthesis, properties and applications," *Chemistry of Materials*, vol. 23, no. 18, pp. 4085–4093, 2011.

[19] E. D. Booth, E. Jones, and B. M. Elliott, "Review of the in vitro and in vivo genotoxicity of dichlorvos," *Regulatory Toxicology and Pharmacology*, vol. 49, no. 3, pp. 316–326, 2007.

[20] E. Evgenidou, K. Fytianos, and I. Poulios, "Semiconductor-sensitized photodegradation of dichlorvos in water using TiO_2 and ZnO as catalysts," *Applied Catalysis B*, vol. 59, no. 1-2, pp. 81–89, 2005.

[21] T. Wu, G. Liu, J. Zhao, H. Hidaka, and N. Serpone, "TiO_2 assisted degradation of dyes IX: photooxidation of asquarylium cyanine dye in aqueous dispersions under visible light irradiation," *Environmental Science and Technology*, vol. 33, no. 9, pp. 1379–1387, 1999.

[22] D. Blake, "Bibliography of work on the heterogeneous photocataloytic removal of hazardous compounds from water and air," Tech. Rep. NREL/TP-510-31319, National Technical Information Service, United States, Department of Commerce, 2001.

[23] W. Wang, J. Zhang, F. Chen, D. He, and M. Anpo, "Preparation and photocatalytic properties of Fe^{3+} Ag@TiO_2 core-shell nanoparticles," *Journal of Colloid and Interface Science*, vol. 323, no. 1, pp. 182–186, 2008.

[24] K. S. W. Sing, D. H. Everett, R. A. W. Haul et al., "Reporting physisorption data for gas/solid interface with special reference to the determination of surface area and porosity," *Pure and Applied Chemistry*, vol. 57, pp. 603–319, 1985.

[25] S. J. Gregg and K. S. W. Sing, *Adsorption, Surface Area and Poracity*, Academic Press, New York, NY, USA, 1982.

[26] J. Yu, J. C. Yu, K.-P. Mitch et al., "Effects of acidic and basic hydrolysis catalysts on the photocatlytic activity and structures of bimodal mesoporous titania," *Journal of Catalysis*, vol. 217, no. 1, pp. 69–78, 2003.

[27] J. Yu, S. Liu, and H. Yu, "Microstructures and photoactivity of mesoporous anatase hollow microspheres fabricated by fluoride-mediated self-transformation," *Journal of Catalysis*, vol. 249, no. 1, pp. 59–66, 2007.

[28] Q. Xiang, J. Yu, and P. K. Wong, "Quantitative characterization of hydroxyl radicals produced by various photocatalysts," *Journal of Colloid and Interface Science*, vol. 357, no. 1, pp. 163–167, 2011.

[29] B. Neppolian, H. C. Choi, S. Sakthivel, B. Arabindoo, and V. Murugesan, "Solar/UV-induced photocatalytic degradation of three commercial textile dyes," *Journal of Hazardous Materials*, vol. 89, no. 2-3, pp. 303–317, 2002.

[30] J. M. Herrmann and C. Guillard, "Photocatalytic degradation of pesticides in agricultural used waters," *Comptes Rendus de l'Académie des Sciences IIC*, vol. 3, no. 6, pp. 417–422, 2000.

[31] H. Li, X. Duan, G. Liu, and L. Li, "Synthesis and characterization of copper ions surface-doped titanium dioxide nanotubes," *Materials Research Bulletin*, vol. 43, no. 8-9, pp. 1971–1981, 2008.

[32] K. Chiang, R. Amal, and T. Tran, "Photocatalytic degradation of cyanide using titanium dioxide modified with copper oxide," *Advances in Environmental Research*, vol. 6, no. 4, pp. 471–485, 2002.

[33] Y. Yang, Q. Wu, Y. Guo, C. Hu, and E. Wang, "Efficient degradation of dye pollutants on nanoporous polyoxotungstate-anatase composite under visible-light irradiation," *Journal of Molecular Catalysis A*, vol. 225, no. 2, pp. 203–212, 2005.